CO Methanation Toward the Production of Synthetic Natural Gas over Highly Active Ni/TiO_2 Catalyst

Vijay M. Shinde and Giridhar Madras
Dept. of Chemical Engineering, Indian Institute of Science, Bangalore 560 012 India

DOI 10.1002/aic.14304
Published online November 28, 2013 in Wiley Online Library (wileyonlinelibrary.com)

The sonochemical synthesis and characterization of highly active and stable Ni nanoparticles supported on TiO_2 as a CO methanation catalyst for the production of synthetic natural gas are reported. The catalyst synthesized by sonication showed higher activity for CH_4 formation than the catalyst synthesized via the conventional wet impregnation method. The activation energy was found to be 79 and 94 kJ mol^{-1} for the catalyst synthesized with sonication and wet impregnation method, respectively. The combined results of x-ray photoelectron spectroscopy and x-ray diffraction show that the enhancement in activity of the sample synthesized by sonication method is due to partial substitution of Ni in TiO_2 lattice. This creates oxide vacancies and facilitates hydrogen adsorption and spillover from nickel to support. H_2-temperature-programmed reduction study corroborates the intimate contact of Ni with support, thus rendering strong metal support interactions. The mechanism involving Langmuir–Hinshelwood kinetics with hydrogen-assisted CO dissociation was used to correlate experimental data. © 2013 American Institute of Chemical Engineers *AIChE J*, 60: 1027–1035, 2014

Keywords: nickel-based catalyst, methanation, synthetic natural gas, kinetic model, coke formation

Introduction

Natural gas, the cleanest fossil fuel, is a highly efficient form of energy because of its high calorific value, smoke, and slag free combustion properties.[1] The increase in demand for natural gas has led one to pursue unconventional methods for the production of synthetic natural gas (SNG). SNG is an artificially produced version of natural gas, which can be obtained from gasification of carbonaceous feedstock (e.g., coal and biomass) to produce CO/H_2 followed its methanation. CH_4 can also be produced via anaerobic digestion of wet biomass (e.g., crops, sewage sludge, and manure). The overall chemical efficiency (energy output of SNG to energy input of biomass) of the former process is about 65% and about 20–40% for the latter process.[2] Thus, the production of SNG via gasification of carbonaceous feedstock and subsequent methanation is an energy efficient process. The formation of tar is one of the major problems associated with this process. However, a suitable catalyst could be used to minimize tar in biomass gasification processes.[3] CO methanation is a key reaction during this transformation. Thermodynamically, this reaction is favored at low temperature but kinetically, this reaction is favored at high temperatures. Therefore, the development of highly active catalyst that is stable against sintering and carbon deposition is desirable.

Metals, such as Ru, Rh, Ni, Co, and so forth on various supports have been reported to be effective methanation catalysts.[4–7] Infrared and other spectroscopic techniques have been used to study the reaction mechanism over Rh supported on various metal oxides (Al_2O_3, SiO_2, and MgO) catalyst. It was found that the rate of dissociation of CO is a rate-controlling step and the low activity of Rh/MgO catalyst is attributed to the low rate constant of the C—O bond dissociation step.[8–10] Ru supported on metal oxides has shown high activity for CO methanation. However, Ru-based catalysts are prohibitively expensive for large-scale applications. However, catalysts based on Ni are relatively active and less expensive, therefore, they are used extensively for industrial applications. Most of aforementioned catalysts are used for selective CO methanation to remove CO from H_2-rich feed gases for fuel cells. However, these catalysts are not suitable for SNG production because the feed for methanation for SNG production contains a large concentration of CO ($H_2/CO > 3$), which makes the overall reaction highly exothermic.[11–13] This leads to the sintering of the active metal and/or support.[14,15] The deactivation of catalyst due to carbon deposition is also dominant at high concentration of CO.[16] Consequently, it is important to develop a stable catalyst with sufficiently high activity at low temperatures and able to suppress both sintering of active metal and deposition of carbon.

Ni supported over various oxides such as Al_2O_3, TiO_2, SiO_2, and SiC[1,6,17,18] have been investigated in the literature. For instance, CO methanation over 10% Ni/Al_2O_3 catalyst was studied using infrared spectroscopy and isotopic techniques, and it was shown that the surface state depends on both the rate of CO dissociation and CH_x hydrogenation without a well-defined rate-determining step.[19] However, the catalytic performance is related to the size, shape of the

Correspondence concerning this article should be addressed to G. Madras at giridhar@chemeng.iisc.ernet.in.

metal nanoparticles, and the interactions between the metals and the supports.[20,21] In general, CO methanation activity is significantly higher for Al_2O_3 supports than SiO_2.[21–23] Therefore, Ni supported on Al_2O_3 catalysts has been explored extensively.[24–26] However, these catalysts are vulnerable to rapid deactivation due to the sintering of Ni particles and carbon deposition at high temperatures.[27,28] Further, the formation of $NiAl_2O_4$ phase at high temperature reduces the CO methanation activity. Although the addition of Al in Pt/CeO_2 catalyst increases the activity for water gas shift reaction, the catalyst is deactivated during the daily start-up and shut-down operation due to the formation of stable carbonate on the surface.[29]

Conversely, several authors have reported the beneficial effect of TiO_2 as support for CO methanation. For example, the specific activity of various Pd-supported catalysts increased in the order of $Pd/SiO_2 << Pd/SiO_2/Al_2O_3 < Pd/Al_2O_3 < Pd/TiO_2$ for CO methanation.[20] The increase in activity is attributed to strong interaction between the active metal and the support. Erdöhelyi et al.[30] have reported that the rate of CH_4 formation over Pd/TiO_2 catalyst was two orders of magnitude higher than that observed for Pd/MgO. The increase in activity is due to the ease of dissociation of adsorbed CO over Pd/TiO_2 catalyst due to electronic interactions between TiO_2 and Pd. However, these interactions are lower over Pd/Al_2O_3. Therefore, the nature of the support may play a crucial role in the reaction mechanism and TiO_2 was found to be a more active support for CO methanation. Recently, it has been shown that the preparation conditions, such as nickel precursors, calcination and reduction temperatures, and nickel content affect the CO methanation activity over Ni/TiO_2 catalysts.[31]

In this study, we have investigated the performance of Ni supported on TiO_2 catalyst synthesized by sonication for the production of SNG via CO methanation. The catalyst was synthesized by low temperature sonication and characterized by x-ray diffraction (XRD), transmission electron microscopy (TEM), x-ray photoelectron spectroscopy (XPS), temperature-programmed reduction (H_2-TPR), thermogravimetric analyses (TGA), and Brunauer-Emmett-Teller (BET) surface analyzer techniques. The catalyst synthesized by the sonication technique exhibits much higher activity and selectivity and also exhibits stronger resistance to carbon deposition compared to the catalyst synthesized by conventional wet impregnation. The increase in the activity was attributed to strong metal support interaction, as evidenced by H_2-TPR study. The steady-state kinetics measurement was carried out over a wide range of temperature and a detailed kinetic mechanism was derived to correlate the experimental data.

Experimental

Synthesis and structural characterization

Ni/TiO_2 was synthesized by low-temperature sonication method from the starting materials, titanyl nitrate ($TiO(NO_3)_2$) and $Ni(NO_3)_2{\cdot}6H_2O$ (S.D Fine Chemicals, India), and diethylenetriamine (DETA; S.D Fine Chemicals). A precipitate of titanyl hydroxide was obtained by the controlled hydrolysis of 5 mL of titanium isopropoxide (Alfa Aesar, India) under ice cold (4°C) condition. The precipitate was washed several times with distilled water and then dissolved in 10 mL of nitric acid to obtain a clear solution of titanyl nitrate. Nickel nitrate (2 g) was dissolved in 20 mL water, separately, and both the solutions were mixed together. DETA (5 mL) was added to the solution which turned into a gel immediately and the resulting solution was irradiated with an ultrasonic probe (125 W) equipped with a Ti-horn of 25-mm diameter for 6 h. The temperature of solution reached 60°C during sonication. The product was filtered, washed with water-ethanol mixture several times, and dried in hot air oven at 120°C for 3 h. The solid product was further heated at 400°C in N_2 for 1 h to remove (if any) the possibility of surface nitrates. The sample containing various % of Ni (8, 15, and 23) over TiO_2 was prepared.

Ni metal (23%) impregnated on TiO_2 was also prepared via conventional wet impregnation method by reducing the nickel nitrate solution with hydrazine hydrate (80%, S.D Fine Chemicals) over TiO_2 made by the sonication method. In a typical synthesis, 1.5 g of TiO_2 was dispersed in water and 2.22 g of $Ni(NO_3)_2{\cdot}6H_2O$ was added. Hydrazine hydrate was then added drop by drop to the mixture to reduce the Ni^{2+} ion in $Ni(NO_3)_2{\cdot}6H_2O$ to Ni metal. After stirring for 30 min, the mixture was filtered and dried at 120°C for 3 h. The resulting dried solid was further heated at 400°C for 1 h in N_2. The catalyst synthesized via sonication method is denoted as 23% Ni/TiO_2 (sonic), whereas the catalyst synthesized via impregnation method is denoted as 23% Ni/TiO_2 (imp).

XRD patterns were recorded on a Philips X'Pert diffractometer using Cu Kα radiation ($\lambda = 0.15406$ nm) source, operating at 40 kV and 30 mA. All the catalysts were scanned in the 2θ range from 10° to 80° with a step size 0.02°/min. The particle size of the catalyst was measured by TEM using a FEI Technai 20 operated at 200 kV. A small amount of powder sample (1 mg) was dispersed ultrasonically in ethanol (4 mL) for 20 min and the suspension was deposited on a carbon coated copper grid (300 mesh) for TEM study. XPS was used to determine the oxidation state of metal cations in the catalyst. The spectra were recorded with a Thermo Scientific Multilab 2000 instrument using Al Kα radiation as an excitation source. The binding energy scale was calibrated by the adventitious carbon (C1s peak at 285 eV). The BET surface area of sample was measured by N_2 adsorption at 77 K, using a surface area analyzer (Smartsorb 93, Smart Instruments Company, India). The sample was degassed at 120°C for 4 h prior to the measurement. TGA were performed in a Mettler Toledo thermal analyzer under pure O_2 flowing rates of 20 mL min^{-1}. Sample (10 mg) was loaded onto the thermobalance and heated to 1000°C at a rate of 10°C min^{-1}.

Temperature programmed reduction

The intimate contact between Ni and TiO_2 was investigated by H_2-TPR study. H_2-TPR study was performed in a quartz tube of 4-mm diameter with a 25-mg sample. The catalyst was preheated at 400°C for 30 min in air and cooled to room temperature (26°C) in the flow of pure Ar. TPR was carried out in the range of 40–500°C at a rate of 10°C min^{-1} in a stream of 5% H_2/Ar gas mixture flowing at a rate of 30 mL min^{-1}. The H_2 consumption during the reduction was measured using a thermal conductivity detector (TCD).

CO methanation activity

The catalytic activity measurement was performed at atmospheric pressure in a tubular quartz reactor (4-mm ID and length of 30 cm) over 0.5 g of catalyst (40–80 mesh)

diluted with 2 g of quartz sand (50–100 mesh). A K-type thermocouple was inserted in direct contact with the catalyst bed to measure the catalyst temperature. Prior to the measurement, the catalyst was reduced at 450°C in pure H_2 flowing at 30 mL min^{-1} for 2 h. The pure H_2 stream was then switched to N_2, and the sample was cooled to room temperature (26°C). Finally, it was tested over a temperature range of 100–440°C. The gas mixtures consisting of 1 vol % of CO, 4 vol % of H_2, and balance of N_2 with total flow rate of 100 mL min^{-1} were fed to the reactor. A ratio of $H_2/CO = 4$ was used because the gasification of the biomass normally leads to streams with $H_2/CO > 3$. This corresponds to gas hour space velocity (GHSV) of 38,800 h^{-1}. The composition of the effluent gas was analyzed on line with a gas chromatograph (Mayura Analytical, Bangalore) equipped with TCD and FID (incorporating a methanator) detectors. The steady-state experiments were performed at various temperatures, and the catalytic activity was measured from the CO conversion (X_{CO}). The selectivity for CH_4 (S_{CH_4}) was calculated from the ratio between CH_4 formation and CO consumption, as a function of reaction temperature. The yield of CH_4 was defined as $Y_{CH_4} = X_{CO} S_{CH_4} \times 100$. The selectivity of CH_4 is not 100% due to the occurrence of Boudouard and water gas shift reaction at higher temperatures. The selectivity for CO_2 can be calculated as the ratio of CO_2 formation to CO consumption.

Results and Discussion

Structural studies

Figure 1 shows the XRD patterns of various Ni-supported TiO_2 catalysts. In 23% Ni/TiO_2 (sonic), the diffraction peaks due to NiO, Ni metal, and rutile TiO_2 were found. However, 23% Ni/TiO_2 (imp) catalyst shows a hump at $2\theta = 44.5°$ due to Ni (111) along with anatase phase of TiO_2. The peaks corresponding to the rutile phase of TiO_2 and NiO were not observed in the XRD pattern. The XRD pattern of 15 % Ni/TiO_2 is also shown in Figure 1a. No peak corresponding to either Ni metal or Ni oxide was observed. Further, close observation of XRD patterns indicate that the observed peak of TiO_2 phase at 27.6° shifted to higher values by 0.5° (due to decrease in d-spacing). The reduction in the lattice parameter of TiO_2 indicates possible ionic substitution of Ni in TiO_2 during the synthesis. Therefore, the solid solution of 15 % Ni/TiO_2 is represented as $Ti_{0.85}Ni_{0.15}O_{2-\delta}$. The XRD pattern was refined using JANA 2000 suite program. The profile was fitted with Pseudo-Voigt as peak shape function and Legendre polynomial (number of terms = 15) as background function. The symbols in the Figure 1b show the observed XRD pattern and the solid lines show the predicted XRD pattern for 23% Ni/TiO_2. The difference between the observed and predicted pattern is also shown at the bottom of Figure 1b. The lattice parameters of 23% Ni/TiO_2 (sonic) are found to be 4.5741 and 2.9389 Å. A decrease in the lattice parameter of 23% Ni/TiO_2 (sonic) compared to unsubstituted TiO_2 indicates the partial substitution of smaller Ni^{2+} ions for larger Ti^{4+} ions in the TiO_2 lattice. The crystallite size of Ni was calculated from full-width half maximum of the peak at 44.5° using Scherrer equation and was found to 16 and 21 nm, respectively, for 23% Ni/TiO_2 (sonic) and 23% Ni/TiO_2 (imp). However, calculation of Ni size of 8 and 15% Ni loading is not possible due to formation of solid solution of Ni and TiO_2. The shape factor (K) used in the Scherrer equation was 0.94 and uncertainty associated with the measurement is ±3 nm. This was further corroborated with TEM analysis.

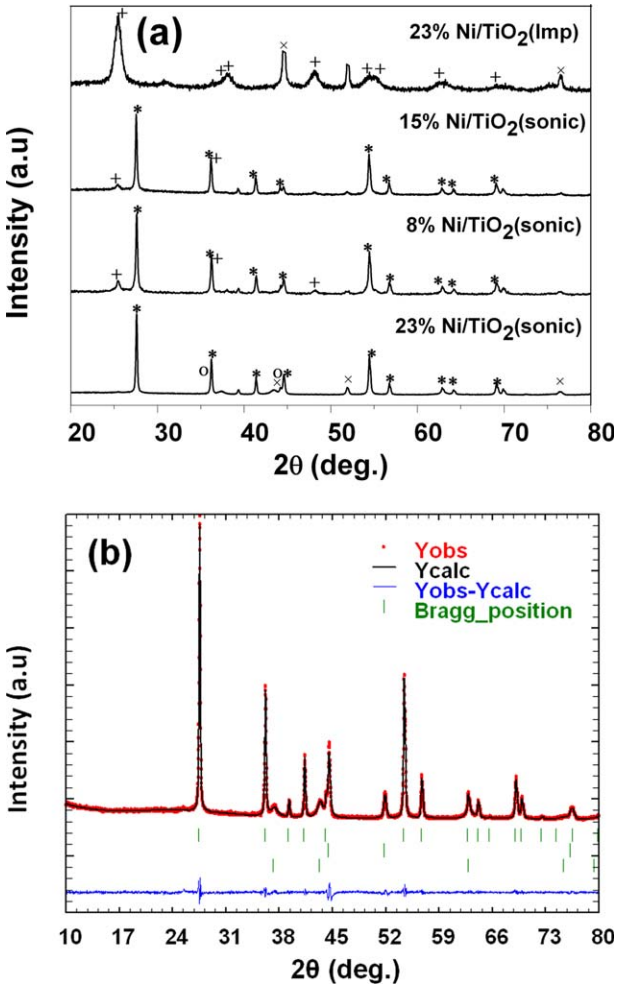

Figure 1. (a) XRD of various Ni-modified TiO_2 catalysts and (b) profile refinement of 23% Ni/TiO_2 (sonic).

[Color figure can be viewed in the online issue, which is available at wileyonlinelibrary.com.]

The bright field image of Ni-supported TiO_2 nanoparticles shows uniformly dispersed spherically shaped particles over the support, synthesized by sonication method (Figure 2a). In contrast, Ni particles synthesized by conventional wet impregnation method tend to agglomerate and form large nanoparticles compared to sonication method. It is also observed from TEM image that the dispersion of Ni particles in conventional wet impregnation method is not uniform over the support. The average particle size of Ni is about 13 and 21 nm, respectively, for 23% Ni/TiO_2 (sonic) and 23% Ni/TiO_2 (imp) catalysts. The Ni content for both the samples was also determined using EDX analysis (not shown here) and was found to be 22 and 27wt %, respectively, for 23% Ni/TiO_2 (sonic) and 23% Ni/TiO_2 (imp) catalysts. Therefore, the sonication method produces the nanoparticles with fine dispersion with large amounts of low-coordinated sites. This activates the reactants at the metal support interface more effectively than the conventional wet impregnation method. The BET surface areas for 23% Ni/TiO_2 (sonic) and 23% Ni/TiO_2 (imp) are 56 and 64 m^2 g^{-1}, respectively. The

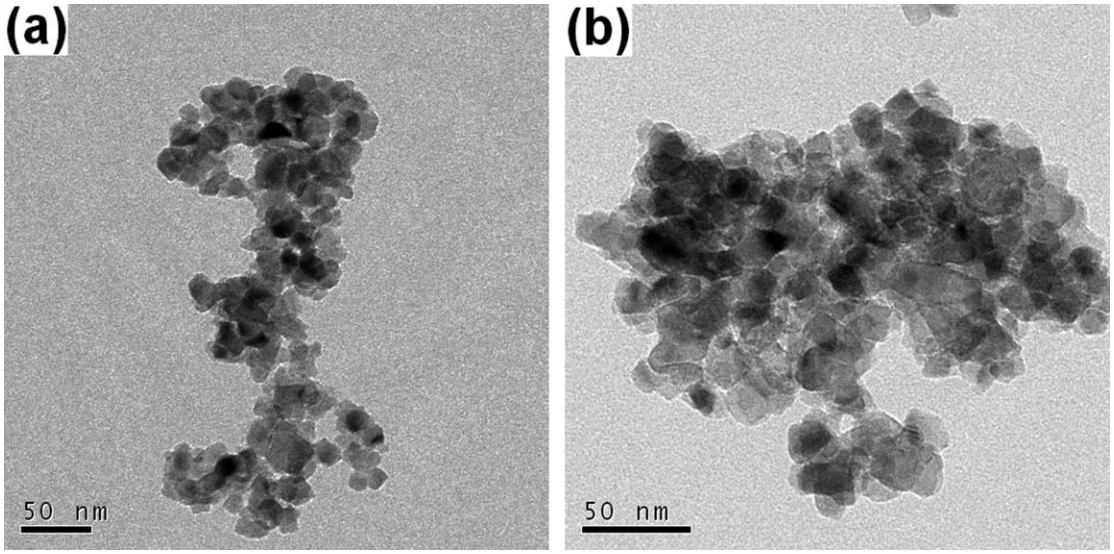

Figure 2. Bright field image for (a) 23% Ni/TiO_2 (sonic) and (b) 23% Ni/TiO_2 (imp), respectively.

surface areas of both the samples after the reaction were measured and no change in the surface areas was observed for both the samples.

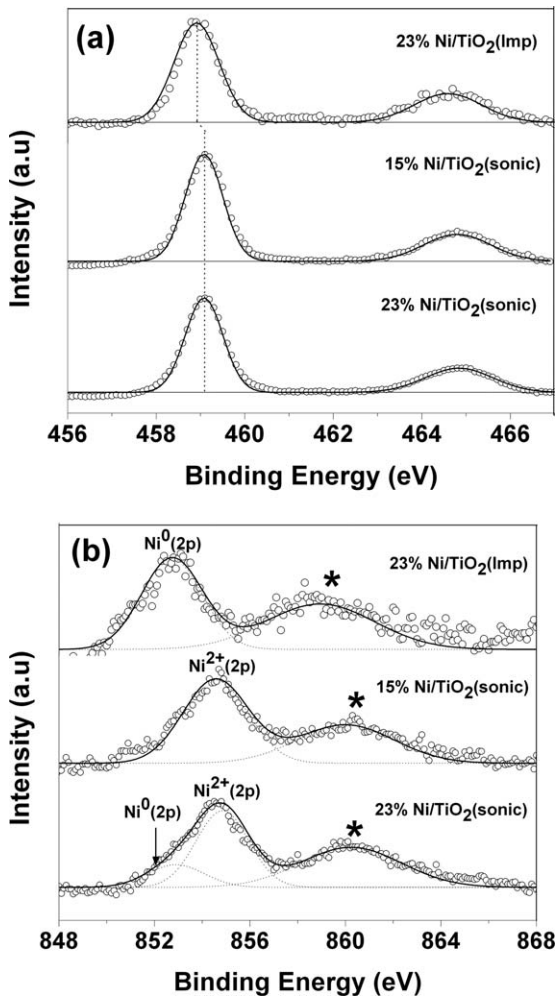

Figure 3. Core level XPS of (a) Ti 2p and (b) Ni 2p of various Ni-modified TiO_2 catalysts.

The nature of interactions between the Ni and the support was investigated by XPS. The partial ionic substitution of Ni^{2+} was also confirmed by XPS. The Ti (2p) spectra in 23% Ni/TiO_2 (sonic), $Ti_{0.85}Ni_{0.15}O_{2-\delta}$, and 23% Ni/$TiO_2$ (imp) catalysts are shown in Figure 3a. The binding energies were calibrated with respect to the binding energy of graphite observed at 284.5 eV. Ti ($2p_{3/2}$) binding energies in all Ni-modified compounds are at ~458.9 eV corresponding to Ti in the 4+ state.[32] However, a slight shift of ~0.2 eV toward higher binding energy was observed for $Ti_{0.85}Ni_{0.15}O_{2-\delta}$ and 23% Ni/TiO_2 (sonic) samples. This shift may be due to the formation of Ti—Ni bond during synthesis.

The core level spectra of Ni (2p) in 23% Ni/TiO_2 (sonic) and 23% Ni/TiO_2 (imp) catalysts are shown in Figure 3b. The XPS spectrum of 23% Ni/TiO_2 (sonic) is broad indicating multiple oxidation states of Ni. Therefore, the main Ni (2p) peak was deconvoluted corresponding to the Ni^{2+} and Ni^0 states. Ni ($2p_{3/2}$) binding energy at 854.6 eV along with the broad satellite at around 860 eV is characteristic of NiO species and the spectrum corresponding to Ni^0 metal is characterized by a peak at a binding energy of 852.6 eV.[33,34] Therefore, Ni is present in mixed oxidation state in 23% Ni/TiO_2 (sonic) catalyst. However, the nickel spectrum is different for 23% Ni/TiO_2 (imp) catalyst. A peak observed at about 852.6 eV was assigned to metallic Ni. The peak corresponding to nickel oxide was not observed on the surface. Therefore, dispersed Ni over 23% Ni/TiO_2 (imp) catalyst surface is metallic in nature. Further, the presence of Ni^{2+} species and a slight shift to higher binding energy for Ti^{4+} species indicate ionic substitution of Ni in $Ti_{0.85}Ni_{0.15}O_{2-\delta}$.

The combined XRD and XPS studies show that Ti was observed in 4+ state in all Ni-modified TiO_2. The aliovalent substitution of Ni^{2+} in the TiO_2 creates oxide ion vacancies to maintain the electrostatic neutrality of the lattice. These oxygen vacancies act as active sites for chemisorption of H_2.[35] Therefore, the oxide ion vacancies provide additional hydrogen adsorption sites, which results in high CO methanation activity for Ni/TiO_2 (sonic). This is further discussed in the activity test section.

H_2-TPR study

Figure 4 shows the H_2-TPR profiles for 23% Ni/TiO_2 (sonic) and 23% Ni/TiO_2 (imp) catalysts. The reduction was

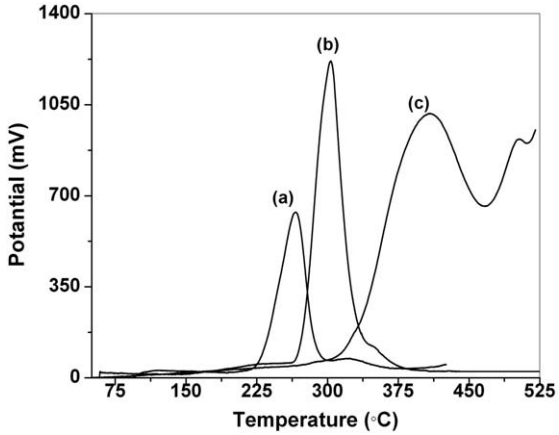

Figure 4. H_2-TPR profile for (a) 23%Ni/TiO_2 (imp), (b) 23%Ni/TiO_2 (sonic), and (c) nickel oxide.

observed for both Ni-supported catalysts over a range of 260–400°C. Pure NiO shows a reduction temperature of about 408°C (see Figure 4). Therefore, the reduction peak between 260 and 400°C was assigned to the reduction of Ni^{2+} species with the significant interaction with TiO_2.[36] The reduction peaks of 23% Ni/TiO_2 (sonic) have a similar profile with those of 23% Ni/TiO_2 (imp). However, 23% Ni/TiO_2 (sonic) shows the reduction at higher temperature compared to 23% Ni/TiO_2 (imp). A known weight of CuO sample was used to calibrate the hydrogen intake/consumption during reduction. The peak area for the reduction of 23% Ni/TiO_2 (sonic) is much higher than that of 23% Ni/TiO_2 (imp). H/Ni ratio was also calculated assuming complete oxidation of Ni for both the catalysts and this was found to be 2.94 and 2.12, respectively, for 23% Ni/TiO_2 (sonic) and 23% Ni/TiO_2 (imp) ($\leq$400°C). The ratio H/Ni >2 indicates that a hydrogen spillover from nickel species to neighboring Ti^{4+} ions is comparatively higher for 23% Ni/TiO_2 (sonic) than 23% Ni/TiO_2 (imp). This indicates that H_2 molecules dissociated on the Ni atom migrated to the support during the reduction of the catalyst.[37] Therefore, the enhancement in the CO methanation activity for 23% Ni/TiO_2 catalyst is mainly due to the stronger interaction exhibited by 23% Ni/TiO_2 (sonic) catalyst. This is further discussed in detail in the activity test section.

Activity test

The variation of CO conversion, CH_4 selectivity, and CH_4 yield with temperature for various Ni-modified TiO_2 catalysts are shown in Figure 5. The yield and selectivity of methane increase with temperature and then decrease with further increase in temperature. The decrease in the yield of CH_4 at higher temperature is due to simultaneous occurrence of CO methanation, Boudouard ($2CO \leftrightarrow CO_2 + C$) and water gas shift ($CO + H_2O \leftrightarrow H_2 + CO_2$) reactions. CO conversion (48%) with 97% CH_4 selectivity was obtained at 320°C over 8% Ni/TiO_2 (sonic) catalyst, whereas 69% CO conversion with 93% CH_4 selectivity was obtained at 320°C over 15% Ni/TiO_2 (sonic) catalyst. The yield of CH_4 is 47 and 64%, respectively, for 8% Ni/TiO_2 (sonic) and 15% Ni/TiO_2 (sonic) catalyst. These catalysts showed lower CO methanation yield than 23% Ni/TiO_2 (sonic) catalyst. Therefore, only 23% Ni/TiO_2 (sonic) catalyst was extensively used for further catalytic studies. In addition, the performance of 8 and 15% Ni/TiO_2 (imp) catalysts was also compared with corresponding to wt % of Ni/TiO_2 (sonic) catalysts. It was found that the activity of sonochemical-synthesized catalyst is always higher than that of catalyst synthesized via conventional impregnation method. At 320°C, the conversion obtained with the impregnated catalysts were 10–15% lower than that of the conversion obtained by the catalysts prepared by sonication. Nearly complete CO conversions (~99%) with 88% CH_4 selectivity were obtained at 320°C over 23% Ni/TiO_2 (sonic) catalyst and 75% CO conversion with 92% CH_4 selectivity was obtained at 340°C over 23% Ni/TiO_2 (imp) catalyst. The yield of CH_4 is 87 and 69%, respectively, for 23% Ni/TiO_2 (sonic) and 23% Ni/TiO_2 (imp) catalysts. Therefore, CH_4 yield over 23% Ni/TiO_2 (sonic) is much higher than that obtained over the 23% Ni/TiO_2 (imp) catalyst. This indicates that 23% Ni/TiO_2 (sonic) catalyst exhibits higher activity than the impregnated catalyst. The higher methanation activity of 23% Ni/TiO_2 (sonic) catalyst is attributed to strong metal support interactions, as evidenced from H_2-TPR. It also shows that the extent of hydrogen spillover from Ni species to neighboring Ti^{4+} ions

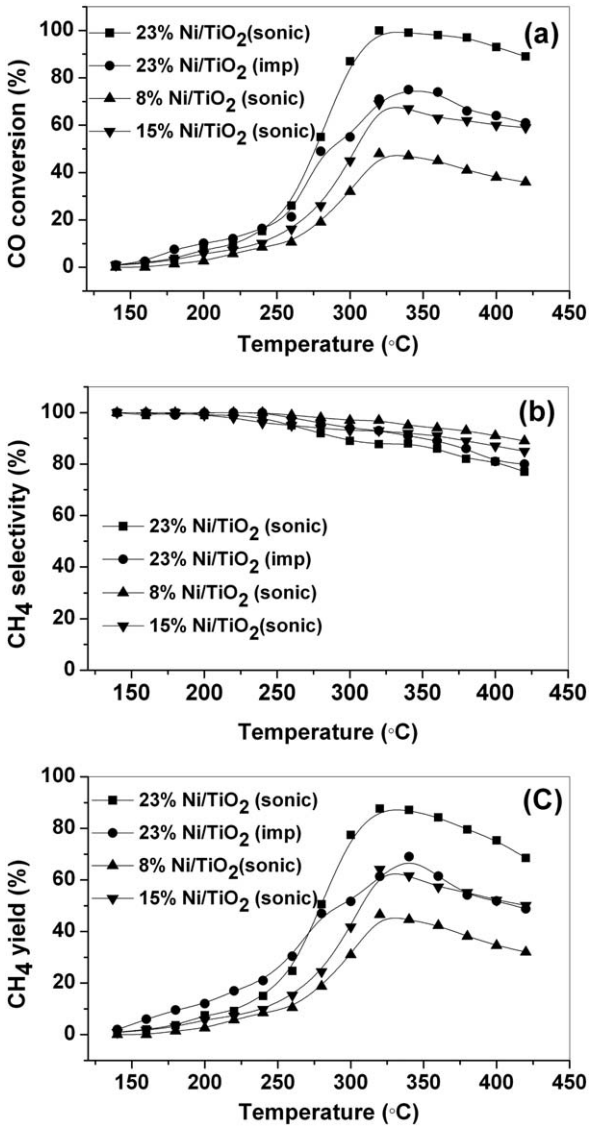

Figure 5. Percentage (a) CO conversion, (b) CH_4 selectivity, and (c) CH_4 yield plot on various TiO_2-modified catalysts.

is larger in the case of 23% Ni/TiO_2 (sonic) as compared to 23% Ni/TiO_2 (imp).

In addition, the XRD study shows that partial ionic substitution of Ni is indeed possible in TiO_2. The substitution of smaller Ni cation (ionic radius) for Ti cation can create both short and long metal cation-oxygen anion bonds. The oxygen atoms bounded to the metal with long bonds is weaker and this increases the reducibility of TiO_2. Further, the aliovalent substitution of Ni perturbs the stoichiometry of supports and creates defects (oxygen vacancies). Göpel et al.[35] showed that adsorption of H_2 is possible in the presence of surface defects and these surface defects act as active sites for the chemisorption of H_2. Further, the oxide vacancies also enhance the O_2 and H_2 storage capacities of catalyst.[35] Therefore, oxide vacancies provide additional sites for H_2 adsorption and the higher activity of 23% Ni/TiO_2 (sonic) catalyst can be understood in terms of less competitive hydrogen adsorption on the nickel surface.[32] The oxide ion vacancies lead to significantly higher H_2 coverage on the support and thus leads to higher activity of 23% Ni/TiO_2 (sonic) catalyst.[38]

The rate and activation energy for CO methanation over 23% Ni/TiO_2 (sonic) catalyst was determined using the differential reactor. The experiments were performed with different weights of the catalyst keeping the total gas flow and GHSV constant. The conversion of CO to CO_2 was negligible (<1%) compared to conversion of CO to methane, in all cases. Therefore, the methanation activity can be calculated either from CO conversion or CH_4 concentration in the effluent stream. The rate was determined using the following equation

$$\text{Rate}\,(r) = \frac{F \times x}{W} = \frac{x}{W/F} \tag{1}$$

where F is the flow of the gas in mol s^{-1}, W is the weight of the catalyst in g, and x is the fractional CO conversion. The variation of fraction conversion (x) with W/F is plotted in Figure 6a. The W/F plot is linear up to ~18% conversion and the rates of reaction were calculated, at various temperatures, from the slope of linear portion. The variation of the rate of reaction with temperature is shown in Figure 6b. The Arrhenius plot is shown in the inset of Figure 6b, and the activation energy was found to be 79 kJ mol^{-1}, which is lower compared to the catalyst synthesized via impregnation method (94 kJ mol^{-1}).

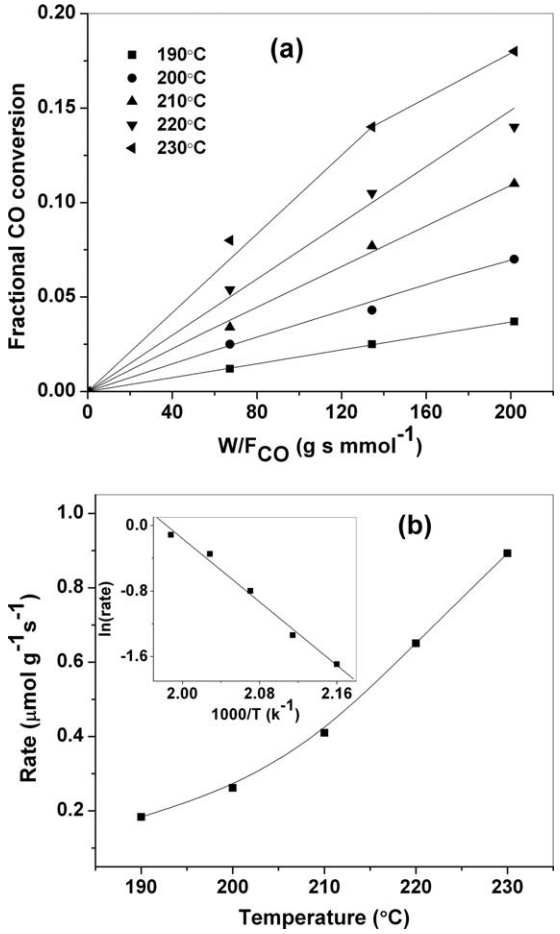

Figure 6. (a) Variation of fractional conversion of CO with W/F_{CO} and (b) rate of reaction as function of temperature along with the Arrhenius plot in the inset, respectively, for Ni/TiO_2.

Kinetic model

The mechanism of CO methanation reaction has been extensively studied. However, it is not understood which of the adsorbed species on the catalyst surface are active and determine CO methanation activity. Two completely different pathways, namely "dissociative pathway" and "hydrogen assisted pathway," have been proposed to describe the reaction kinetics.[20,39,40] The "dissociative pathway" involves hydrogenation of surface carbon produced by dissociative adsorption of CO, whereas the "hydrogen assisted pathway" involves direct hydrogenation of adsorbed CO species.[17] The debate is whether the reaction initiates with direct CO dissociation or hydrogen-assisted CO dissociation. It has been proposed that CO dissociates in the initial step leading to two types of carbon species, namely active and inactive. Then, the former type is stepwise methanated to CH_4 through various adsorbed intermediate species, such as CH, CH_2, and CH_3.[41,42] However, transient experiments have shown that these adsorbed CH_x species represent side products rather than the reaction intermediates.[43,44]

In another study, it has been indicated that a formyl-type (HCO) species plays an important role in the CO methanation reaction, followed by C—O bond breaking, and further hydrogenation.[45] This formyl-type intermediate was also identified in the dominant reaction pathway using density functional theory (DFT) calculation.[46,47] It has been shown that the HCO species was formed during the reaction of adsorbed CO with atomic hydrogen over Ru (001) at 100 K.[48] They have shown that, experimentally and theoretically, different surface species are favorable (HCO or COH) over Ni surfaces and depend on the nature of Ni sites and partial pressure of CO.[45] However, H-assisted CO dissociation is more facile than direct CO dissociation. DFT calculation was used to trace the methanation reaction and it has been shown that the reaction proceeds via the H-assisted CO dissociation reaction through the formyl species.[49] It should be noted that the mechanism of CO methanation reaction may include both dissociative and associative paths. The predominance of one path over other depends on the catalyst and experimental conditions used.[50]

Based on the above discussion, a kinetic model for CO methanation was proposed over Ni-supported TiO_2. The

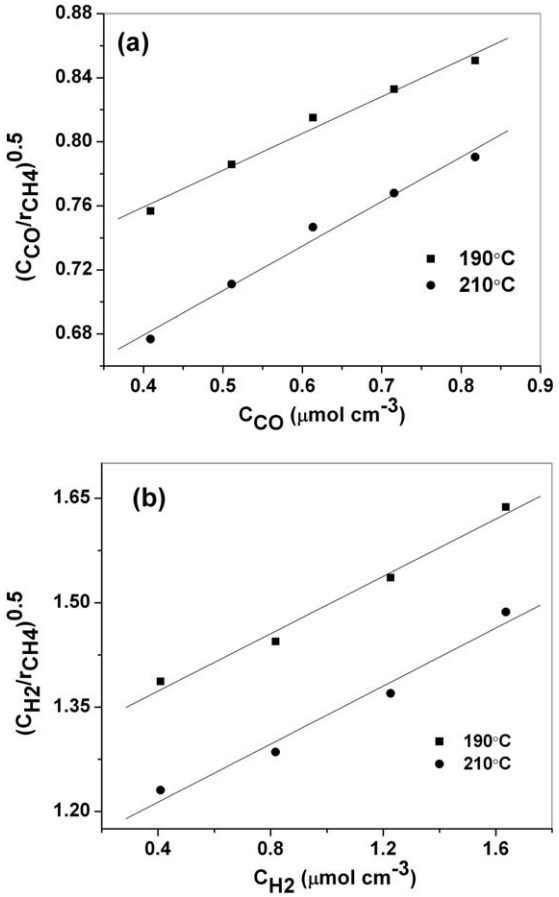

Figure 7. Fitted rate of CO methanation to kinetic model as function of concentration of (a) C_{CO} and (b) C_{H_2}.

model assumes that the adsorbed CO strongly interacts with adsorbed hydrogen

$$CO + M \overset{K_1}{\leftrightarrow} CO - M \tag{2}$$

$$H_2 + 2M \overset{K_2}{\leftrightarrow} 2H - M \tag{3}$$

$$CO - M + 2H - M \xrightarrow{k_3} C - M + H_2O \tag{4}$$

$$C - M + H - M \xrightarrow{k_4} CH - M + M \tag{5}$$

$$CH - M + H - M \xrightarrow{k_5} CH_2 - M + M \tag{6}$$

$$CH_2 - M + H - M \xrightarrow{k_6} CH_3 - M + M \tag{7}$$

$$CH_3 - M + H - M \xrightarrow{k_7} CH_4 + 2M \tag{8}$$

There is no evidence in the literature that methanation requires a dual functional catalyst. Therefore, Eqs. 2 and 3 show that adsorbed CO and H_2 over Ni sites is in equilibrium with gas-phase CO and H_2, respectively. The hydrogen-assisted CO dissociation is represented by Eq. 4. In addition, if we assume direct dissociation of CO pathway as the rate-determining step is operative over the present catalyst, the rate of reaction should be independent of H_2 partial pressure. However, our results clearly show that the rate of reaction increases with partial pressure of H_2.

Coenen et al.[51] have not observed isotopic scrambling when $^{13}C^{16}O$ and $^{12}C^{18}O$ are together with hydrogen, indicating hydrogen or nonhydrogen-assisted CO dissociation is the rate-determining step. The DFT was used to calculate energies of transition states and the stable intermediates in reforming over the closed packed Ni (111) and the stepped Ni (211) sites and the highest energy barrier was found for the CO dissociation step.[52] These results can be used to obtain information about the present reaction because reforming is the reverse reaction of CO methanation. Therefore, in deriving the kinetic expression, it was explicitly assumed that hydrogen-assisted CO dissociation step (Eq. 4) is the rate-limiting step and hydrogenation of the CH_x species leading to the formation of CH_4 was assumed to be very fast (Eqs. 5–8). Further, no assumptions regarding CO coverage was made and formation of CH_4 take place from surface carbon produced by hydrogen-assisted CO dissociation step. Solving the above set of elementary steps, we obtain the rate expression as

$$r_{CH_4} = \frac{K_1 K_2 k_3 C_{CO} C_{H_2}}{(1 + K_1 C_{CO} + K_2 C_{H_2})^2} \tag{9}$$

At constant partial pressure of H_2, Eq. 9 can be rewritten as

$$r_{CH_4} = \frac{A \times C_{CO}}{(B \times C_{CO} + D)^2} \tag{10a}$$

where $A = K_1 K_2 k_3 C_{H_2}$, $B = K_1$, and $D = (1 + K_2 C_{H_2})$

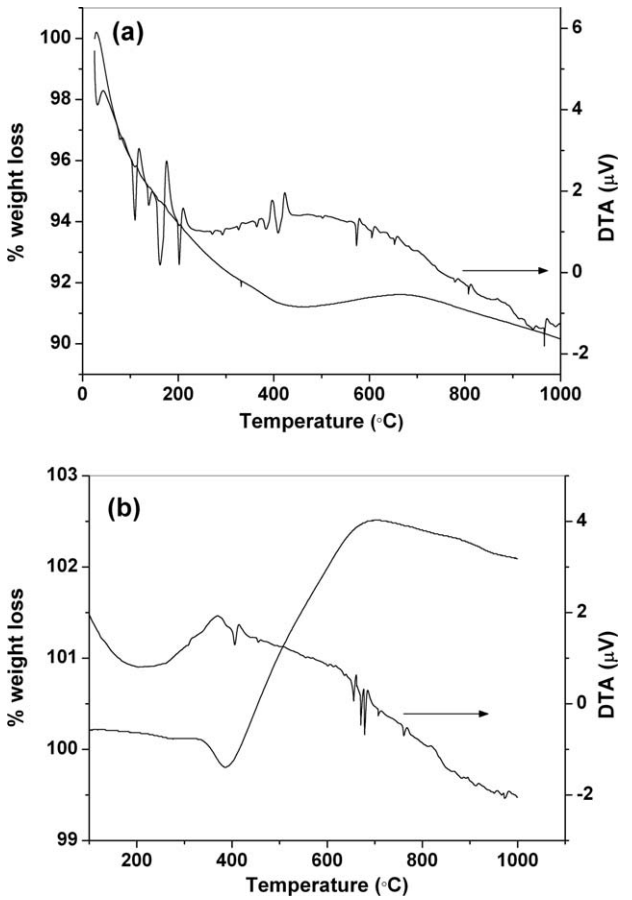

Figure 8. TGA-DTA plot for (a) 23% Ni/TiO_2 (sonic) and (b) 23% Ni/TiO_2 (imp) catalysts, respectively, under pure oxygen after 70 h on stream.

At constant partial pressure of CO, Eq. 9 can be rewritten as

$$r_{CH_4} = \frac{A' \times C_{H_2}}{(B' \times C_{H_2} + D')^2} \quad (10b)$$

where $A' = K_1 K_2 k_3 C_{CO}$, $B' = K_1$, and $D' = (1 + K_2 C_{CO})$

Further, Eqs. 10a and 10b can be rearranged as

$$\left(\frac{C_{CO}}{r_{CH_4}}\right)^{\frac{1}{2}} = \frac{B}{A^{\frac{1}{2}}} + \frac{D}{A^{\frac{1}{2}}} C_{CO} = E + F \times C_{CO} \quad (11a)$$

$$\left(\frac{C_{H_2}}{r_{CH_4}}\right)^{\frac{1}{2}} = \frac{B'}{A'^{\frac{1}{2}}} + \frac{D'}{A'^{\frac{1}{2}}} C_{H_2} = E' + F' \times C_{H_2} \quad (11b)$$

Two sets of experiments were conducted. In the first set, the partial pressure of H_2 was kept constant and the partial pressure of CO was varied. In the second set, the partial pressure of CO was kept constant and the partial pressure of H_2 was varied. The total feed flow rate and catalyst loading were kept constant at 100 $cm^3\ min^{-1}$ and 100 mg. The fit of left side of Eq. 10a with partial pressure of CO resulted in straight line and the values of E' and F' were determined from the intercept and slope, respectively. A similar fit was obtained with the variation of partial pressure of H_2 and values of K_1, K_2, and k_3 were determined (see Figures 7a, b). The values for K_1 ($cm^3\ mol^{-1}$), K_2 ($cm^3\ mol^{-1}$), and k_3 (mol $g^{-1}\ s^{-1}$) are 1.5×10^5 exp (4360/T), 9.6×10^3exp (3040/T), and 5.1×10^4exp (−4780/T), respectively. The mechanism involving direct CO dissociation as a rate-determining step and its subsequent hydrogenation into CH_4 was also considered. The corresponding kinetic expression was derived and used to fit the experimental data. However, good fitting to the experimental data was not obtained. Therefore, hydrogenation of surface carbon produced by dissociative adsorption of CO is the main reaction pathway.

Coke deposition

Ni-based catalysts are vulnerable to deactivation due to carbon deposition. Therefore, TGA in the presence of pure O_2 was used to estimate the carbon deposition over the catalyst surface. The TGA-DTA plots for both the catalysts after 70 h are presented in Figure 8. In both catalysts, the initial weight loss was observed in the range of 150–300°C, which is ascribed to thermal desorption of H_2O and adsorbed CO_2 and removal of formate/carbonate species.[53] The weight of both the used catalysts increased at 400–600°C because of the oxidation of Ni to NiO, and the oxidation of coke to CO and CO_2 occurred mainly above 650°C. The increase in weight is higher for 23% Ni/TiO_2 (imp) compared to 23% Ni/TiO_2 (sonic) catalyst, indicating the former is in more reduced state. The weight loss above 650°C is 1.46 and 0.41%, respectively, for 23% Ni/TiO_2 (imp) and for 23% Ni/TiO_2 (sonic) catalysts, indicating the coke deposition is high over the 23% Ni/TiO_2 (imp) catalyst. The resistance to carbon formation over 23% Ni/TiO_2 (sonic) catalyst is attributed to the partial ionic substitution (partial solid solution) of Ni in TiO_2 support. This phenomenon is well-reported for steam and dry reforming reaction over the solid solution of NiO and MgO.[54,55]

Conclusions

The catalyst synthesized by the sonication method exhibited higher activity and stability for CO methanation reaction compared to the catalyst synthesized by wet impregnation. The catalyst synthesized by sonication method showed very fine dispersion of active species. The enhancement in activity and high resistance to coke deposition of the catalyst were attributed to the partial substitution of Ni in TiO_2 lattice that create oxide vacancies. The strong metal support interaction also provides high resistance to carbon deposition. The H_2-assisted CO dissociation was assumed as the rate-determining step and used to correlate experimental data. The present approach to improve the catalytic activity by creation of oxide vacancies for hydrogen dissociation is encouraging in the context of designing novel catalysts with improved catalytic performance for SNG production by CO methanation.

Acknowledgment

Authors gratefully acknowledge the Gas authority of India Limited for financial assistance.

Literature Cited

1. Hu D, Gao J, Ping Y, Jia L, Gunawan P, Zhong Z, Xu G, Gu F, Su F. Ni catalysts enhanced investigation of CO methanation over Ni/Al2O3 catalysts for synthetic natural gas production. *Ind Eng Chem Res*. 2012;51:4875–4886.
2. Kopyscinski J, Schildhauer TJ, Biollaz SMA. Production of synthetic natural gas (SNG) from coal and dry biomass: a technology review from 1950 to 2009. *Fuel*. 2010;89:1763–1783.
3. Shen L, Gao Y, Xiao J. Simulation of hydrogen production from biomass gasification in interconnected fluidized beds. *Biomass Bioenergy*. 2008;32:120–127.
4. Kimura M, Miyao T, Komori S, Chen A, Higashiyama K, Yamashita H, Watanabe M. Selective methanation of CO in hydrogen-rich gases involving large amounts of CO2 over Ru-modified Ni-Al mixed oxide catalysts. *Appl Catal A*. 2010;379:182–187.
5. Panagiotopoulou P, Kondarides DI, Verykios XE. Mechanistic aspects of the selective methanation of CO over Ru/TiO2 catalyst. *Catal Today*. 2012;181:138–147.
6. Yu Y, Jin G, Wang Y, Guo XY. Synthesis of natural gas from CO methanation over SiC supported Ni-Co bimetallic catalysts. *Catal Commun*. 2013;10:5–10.
7. Prieto G, Concepción P, Martínez A, Mendoza E. New insights into the role of the electronic properties of oxide promoters in Rh-catalyzed selective synthesis of oxygenates from synthesis gas. *J Catal*. 2011;280:274–288.
8. Efstathiou AM. The CO/H2 reaction on Rh/MgO studied by transient isotopic methods. *J Mol Catal*. 1991;67:229–249.
9. Efstathiou AM, Bennett CO. The CO/H2 reaction on Rh/Al2O3. I. Steady state and transient kinetics. *J Catal*. 1989;120:118–136.
10. Efstathiou AM, Bennett CO. The CO/H2 reaction on Rh/A12O3. II. Kinetic study by transient isotopic methods. *J Catal*. 1989;120:137–156.
11. Yu Y, Jin GQ, Wang YY, Guo XY. Synthetic natural gas from CO hydrogenation over silicon carbide supported nickel catalysts. *Fuel Process Technol*. 2011;92:2293–2298.
12. Zhao A, Ying W, Zhang H, Ma H, Fang D. Ni-Al2O3 catalysts prepared by solution combustion method for syngas methanation. *Catal Commun*. 2012;17:34–38.
13. Liu Z, Chu B, Zhai X, Jin Y, Cheng Y. Total methanation of syngas to synthetic natural gas over Ni catalyst in a microchannel reactor. *Fuel*. 2012;95:599–605.
14. Rostrup-Nielsen J, Pedersen K, Sehested J. High temperature methanation: sintering and structure sensitivity. *Appl Catal A*. 2007;330:134–138.
15. Agnelli M, Kolb M, Mirodatos C. Co hydrogenation on a nickel catalyst. 1. Kinetics and modeling of a low-temperature sintering process. *J Catal*. 1994;148:9–21.
16. Mirodatos C, Praliaud H, Primet M. Deactivation of nickel-based catalysts during CO methanation and disproportionation. *J Catal*. 1987:107:275–287.
17. Panagiotopoulou P, Kondarides DI, Verykios XE. Mechanistic study of the selective methanation of CO over Ru/TiO2 catalyst: identification of active surface species and reaction pathways. *J Phys Chem C*. 2010;115:1220–1230.

18. Wang Y, Wu R, Zhao Y. Effect of ZrO2 promoter on structure and catalytic activity of the Ni/SiO2 catalyst for CO methanation in hydrogen-rich gases. *Catal Today*. 2010;158:470–474.
19. Stockwell DM, Chung JS, Bennett CO. A transient infrared and isotopic study of methanation over Ni/A12O3. *J Catal*. 1988;112:135–144.
20. Wang S, Moon S, Vannice MA. The effect of SMSI (strong metal-support interaction) behavior on CO adsorption and hydrogenation on Pd catalysts: II. Kinetic behavior in the methanation reaction. *J Catal*. 1981;71:167–174.
21. Bracey J, Burch R. Enhanced activity of PdTiO2 catalysts for the CO-H2 reaction in the absence of strong metal-support interactions (SMSI). *J Catal*. 1984;86:384–391.
22. Vannice MA. The catalytic synthesis of hydrocarbons from H2/CO mixtures over the group VIII metals. *J Catal*. 1975;37:462–473.
23. Kim MY, Ha SB, Koh DJ, Byun C, Park ED. CO methanation over supported Mo catalysts in the presence of H_2S. *Catal Commun*. 2013;35:68–71.
24. Fujita SI, Takezawa N. Difference in the selectivity of CO and CO2 methanation reactions. *Chem Eng J*. 1997;68:63–68.
25. Mok Y, Kang HC, Lee HJ, Koh D, Shin D. Effect of nonthermal plasma on the methanation of carbon monoxide over nickel catalyst. *Plasma Chem Plasma Process*. 2010;30:437–447.
26. Czekaj I, Loviat F, Raimondi F, Wambach J, Biollaz S, Wokaun A. Characterization of surface processes at the Ni-based catalyst during the methanation of biomass-derived synthesis gas: X-ray photoelectron spectroscopy (XPS). *Appl Catal A*. 2007;329:68–78.
27. Ma S, Tan Y, Han Y. Methanation of syngas over coral reef-like Ni/Al2O3 catalysts. *J Nat Gas Chem*. 2011;20:435–440.
28. Struis RPWJ, Schildhauer TJ, Czekaj I, Janousch M, Biollaz S, Ludwig C. Sulphur poisoning of Ni catalysts in the SNG production from biomass: a TPO/XPS/XAS study. *Appl Catal A*. 2009;362:121–128.
29. Shinde VM, Madras G. A single stage water-gas shift reaction over highly active and stable Siand Al substituted Pt/CeO2 catalysts. *ChemCatChem*. 2012;4:1968–1978.
30. Erdöhelyi A, Pásztor M, Solymosi F. Catalytic hydrogenation of CO2 over supported palladium. *J Catal*. 1986;98:166–177.
31. Urasaki K, Tanpo Y, Nagashima Y, Kikuchi R, Satokawa S. Effects of preparation conditions of Ni/TiO2 catalysts for selective CO methanation in the reformate gas. *J Appl Catal A*. 2013;452:174–178.
32. Briggs D, Seah MP, Briggs D, Seah MP. Practical Surface Analysis by Auger and X-Ray Photoelectron Spectroscopy. Chichester: Wiley, 1983.
33. Girault P, Grosseau-Poussard J, Dinhut J, Marechal L. Influence of a chromium ion implantation on the passive behavior of nickel in artificial sea-water: an EIS and XPS study. *Nucl Instrum Methods Phys Res*. 2001;174:439–452.
34. Dissanayake D, Rosynek MP, Kharas KCC, Lunsford JH. Partial oxidation of methane to carbon monoxide and hydrogen over a Ni/Al2O3 catalyst. *J Catal*. 1991;132:117–127.
35. Göpel W, Rocker G, Feierabend R. Intrinsic defects of TiO2 (110): interaction with chemisorbed O2, H2, CO, and CO2. *Phys Rev B: Condens Matter*. 1983;28:3427.
36. Yan Q, Weng W, Wan H, Toghiani H, Toghiani R, Pittman C. Activation of methane to syngas over a Ni/TiO2 catalyst. *Appl Catal A*. 2003;239:43–58.
37. Tada S, Yokoyama M, Kikuchi R, Haneda T, Kameyama H. N2O Pulse titration of Ni/α-Al2O3 catalysts: a new technique applicable to nickel surface area determination of nickel based catalysts. *J Phys Chem C*. 2013;117:14652–14658.
38. Benvenutti BV, Franken L, Moro CC. FTIR study of hydrogen and carbon monoxide adsorption on Pt/TiO_2, Pt/ZrO2, and Pt/Al_2O3. *Langmuir*1999;15:8140–8146.
39. Ojeda M, Nabar R, Nilekar AU, Ishikawa A, Mavrikakis M, Iglesia E. CO activation pathways and the mechanism of Fischer-Tropsch synthesis. *J Catal*. 2010;272:287–297.
40. Cant NW, Bell AT. Studies of carbon monoxide hydrogenation over ruthenium using transient response techniques. *J Catal*. 1982;73:257–271.
41. Gupta NM, Londhe V, Kamble V. Gas-uptake, methanation, and microcalorimetric measurements on the co-adsorption of CO and H2 over polycrystalline Ru and a Ru/TiO2 Catalyst. *J Catal*. 1997;168:423–437.
42. Bonzel H, Krebs H. On the chemical nature of the carbonaceous deposits on iron after CO hydrogenation. *Surf Sci*. 1980;91:499–513.
43. Gupta N, Kamble V, Kartha V, Iyer R, Thampi KR, M. Gratzel. FTIR spectroscopic study of the interaction of CO and CO2+H2 over partially oxidized RuTiO2 catalyst. *J Catal*. 1994;146:173–184.
44. Ekerdt JG, Bell AT. Synthesis of hydrocarbons from CO and H2 over silica-supported Ru: reaction rate measurements and infrared spectra of adsorbed species. *J Catal*. 1979;58:170–187.
45. Andersson M, Abild-Pedersen F, Remediakis I, Bligaard T, Jones G, Engbæk J, Lytken O, Horch S, Nielsen JH, Sehested J. Structure sensitivity of the methanation reaction: H2-induced CO dissociation on nickel surfaces. *J Catal*. 2008;255:6–19.
46. Inderwildi OR, Jenkins SJ, King DA. Fischer-Tropsch mechanism revisited: alternative pathways for the production of higher hydrocarbons from synthesis gas. *J Phys Chem C*. 2008;112:1305–1307.
47. Inderwildi OR, Jenkins SJ, King DA. Mechanistic studies of hydrocarbon combustion and synthesis on noble metals. *Angew Chem Int Ed*. 2008;47:5253–5255.
48. Eckle S, Anfang HG, Behm RJ. Reaction intermediates and side products in the methanation of CO and CO2 over supported Ru catalysts in H2-rich reformate gases. *J Phys Chem C*. 2011;115:1361–1367.
49. Inderwildi OR, Jenkins SJ. In-silico investigations in heterogeneous catalysis-combustion and synthesis of small alkanes. *Chem Soc Rev*. 2008;37:2274–2309.
50. Sachtler J, Kool J, Ponec V. The role of carbon in methanation by cobalt and ruthenium. *J Catal*. 1979;56:284–286.
51. Coenen J, Van Nisselrooy P, De Croon M, Van Dooren P, Van Meerten R. The dynamics of methanation of carbon monoxide on nickel catalysts. *Appl Catal*. 1986;25:1–8.
52. Bengaard HS, Nørskov JK, Sehested J, Clausen B, Nielsen L, Molenbroek A, Rostrup-Nielsen J. Steam reforming and graphite formation on Ni catalysts. *J Catal*. 2002;209:365–384.
53. Tsyganok AI, Tsunoda T, Hamakawa S, Suzuki K, Takehira K, Hayakawa T. Dry reforming of methane over catalysts derived from nickel-containing Mg-Al layered double hydroxides. *J Catal*. 2003;213:191–203.
54. Yamazaki O, Tomishige K, Fujimoto K. Development of highly stable nickel catalyst for methane steam reaction under low steam to carbon ratio. *Appl Catal A*. 1996;136:49–56.
55. Tomishige K, Chen Y, Fujimoto K. Studies on carbon deposition in CO2 reforming of CH4 over nickel-magnesia solid solution catalysts. *J Catal*. 1999;181:91–103.

Manuscript received Aug. 3, 2013, and revision received Sept. 29, 2013.